



HAL
open science

Solvothermal sol-gel synthesis of TiO₂ cellulose nanocrystalline composites

Andrey Zdravkov, Maria Listratenko, Stanislav Gorbachev, Iraida Osovskaya,
Andrei Kanaev, Nikolai Khimich

► **To cite this version:**

Andrey Zdravkov, Maria Listratenko, Stanislav Gorbachev, Iraida Osovskaya, Andrei Kanaev, et al.. Solvothermal sol-gel synthesis of TiO₂ cellulose nanocrystalline composites. Cellulose, 2021. hal-03092629

HAL Id: hal-03092629

<https://hal.science/hal-03092629v1>

Submitted on 2 Jan 2021

HAL is a multi-disciplinary open access archive for the deposit and dissemination of scientific research documents, whether they are published or not. The documents may come from teaching and research institutions in France or abroad, or from public or private research centers.

L'archive ouverte pluridisciplinaire **HAL**, est destinée au dépôt et à la diffusion de documents scientifiques de niveau recherche, publiés ou non, émanant des établissements d'enseignement et de recherche français ou étrangers, des laboratoires publics ou privés.

1 Andrey Zdravkov^a, Maria Listratenko^b, Stanislav Gorbachev^c, Iraidia Osovskaya^c,
2 Andrey Kanaev^d, Nikolai Khimich^b

3

4 **Solvothermal sol-gel synthesis of TiO₂-** 5 **cellulose nanocrystalline composites**

6 *^a Grebenshchikov Institute of Silicate Chemistry, Russian Academy of Sciences,*
7 *Makarova emb. 2, 199034, St. Petersburg, Russian Federation*

8 *^b Kirov Military Medical Academy, Akademika Lebedeva str. 6, 194044, St.*
9 *Petersburg, Russian Federation*

10 *^c St. Petersburg State University of Industrial Technology and Design the Higher*
11 *School Of Technologies and Power Engineering, Ivana Chernykh str. 4, 198095,*
12 *St. Petersburg, Russian Federation*

13 *^d Laboratoire des Science des Procédés et des Matériaux, CNRS, Université*
14 *Sorbonne Paris Nord, 93430, Villetaneuse, France*

15

16

17

18

19

20

21

22

23

24

25

26

27

28

29

30

31

32

33

34 **Abstract**

35 Due to its unique supramolecular structure, cellulose is widely used as a template agent, ensuring
36 an easy structuring of anatase TiO₂ particles with subsequent release after the organics burning.
37 This work is devoted to the synthesis of microcrystalline cellulose-TiO₂ (MCC-TiO₂) composite
38 photocatalyst by preserving the intermediate organic-inorganic structures. A series of the MCC-
39 TiO₂ materials were prepared via solvothermal sol-gel method in n-decane and caproic acid
40 solvents and characterized by X-ray diffraction, transmission electron microscopy, IR
41 spectroscopy, ¹H NMR and TG/DSC methods. The photocatalytic activity of the prepared
42 materials was evaluated by the decomposition of formic acid in aqueous solutions. The composites
43 failed to be formed in n-decane, while in caproic acid, acting as solvent and reagent, anatase TiO₂
44 nanoparticles were formed onto the crystalline domains of cellulose, tightly fixed due to covalent
45 Ti-O-C bonds. The materials formed in caproic acid showed a higher photocatalytic activity,
46 explained by a complementarity of the organic and inorganic components. The specific activity
47 (normalized on TiO₂ mass) of best synthesized composite materials was almost twice higher than
48 that of Aeroxide P25 TiO₂ reference photocatalyst.

49 **Keywords**

50 Microcrystalline cellulose-titania composite; solvothermal synthesis; sol-gel

51 **Introduction**

52 Among different semiconductors (TiO_2 , WO_3 , Fe_2O_3 , SrTiO_3 , ZnO , etc.) that can
53 be used in photocatalytic process for degradation of organic pollutants, TiO_2 has
54 received a particular interest because of its high activity, chemical stability,
55 relatively low cost and low toxicity [Mory 2005; Sharon et al. 2016; Tang et al.
56 2018]. However, the research on the improved photocatalyst design is still under
57 way. Between different approaches, composite materials can be an interesting
58 solution capable affecting charge separation and trapping effectiveness and light
59 absorption efficiency. A striking example of a two-component system of noble
60 metal and semiconductor particles can be given [Zhang et al. 2013], which
61 synergy is based on a Schottky junction and localized surface plasmon resonance.
62 Excellent charge separation efficiency can also take place in composite or hybrid
63 species including inorganic TiO_2 and organic polymer components [Kuznetsov et
64 al. 2009; Gorbovyi et al. 2011]. The synthesis of such materials has overcome
65 numerous problems, related to the preparation of ensembles of freestanding
66 particles, their uniform distribution free of aggregation, and link to the host
67 polymer by strong covalent bonds.

68 Both inorganic (e.g. montmorillonite [Tieng et al. 2011]) and organic (e.g.
69 polyamide-amine-epichlorohydrin [Wang et al. 2015], polylactide [Kaseem et al.
70 2019]) polymers can be taken as complementary components of photocatalytic
71 materials. At the same time, use of natural biopolymer cellulose could be a
72 particularly attractive solution [Dette et al. 2014; Filippo et al. 2015; Sathasivam
73 et al. 2015; He et al. 2016; Butman et al. 2018; Garusinghe et al. 2018;
74 Rahmawati et al. 2017; Wittmar et al. 2015; Oliveira et al. 2017; Shahrezaei et al.
75 2017.; Melvin et al. 2019; Habibi et al. 2020]. Cellulose does not absorb in the
76 UV-visible spectral range [Sirvio et al. 2016] and cannot screen action spectrum
77 of the photoactive TiO_2 component. A very interesting supramolecular structure
78 and multilevel structural organization of this polymer [Farag et al. 2017] explains
79 its wide use as a template agent [Ioelovich 2014; Lu et al. 2013; Wang et al. 2016;
80 Kayaalp et al. 2014; Xiao et al. 2017; Postnova et al. 2015; Zlotski et al. 2017;
81 Shevtsova et al. 2018; Brandes et al. 2016], ensuring an easy structuring of
82 anatase TiO_2 particles. The thermal post-treatment performed in the related studies
83 has resulted in a burnout of the organic component with subsequent formation of
84 anatase nanoparticles with the shape and size control, exhibiting photocatalytic

85 activity [Postnova et al. 2015]. Naturally, cellulose degrades in these conditions
86 leading to the decomposition of the intermediate structures. Attempts to preserve
87 the organic component in the final photocatalyst are rare [Galkina et al. 2014;
88 Khalid et al. 2017; Luo et al. 2014; Morawski et al. 2013; Melvin et al. 2019; Sun
89 et al. 2010]. The synthesis by decomposition of titanium isopropoxide in ethanol
90 media together with wood cellulose fibers in the microwave-assisted solvothermal
91 process has been reported by Cardoso et al. [Cardoso et al. 2018] and the
92 mechanism of the nucleation and growth of TiO₂ nanoparticles on cellulose fibers
93 has been depicted. Although photocatalytic applications were suggested, no
94 evaluation of the material activity has been presented in this study. The
95 photocatalyst preparation via low-temperature sol-gel method has been reported
96 by Morshed et al. [Morshed et al. 2020] and its activity on methylene blue dye
97 decomposition in aqueous solution (pH=6) under UV light resulted in the first
98 order kinetics with rate constant of 0.188 1/min. The material has shown a good
99 stability with negligible deactivation after 5 recycling. Very recently, Li et al. [Li

100 et al. 2020] have realized a controlled synthesis of TiO₂-cellulose nanocomposites
101 via biotemplate method and assigned an enhanced photocatalytic activity to the
102 ligand-to-metal charge transfer complex at the interface between the components.
103 In this study, the material activity has been evaluated on Cr(VI) reduction in
104 particular acid conditions at pH=3 in the visible spectral range of $\lambda \geq 420$ nm and
105 compared with P25 TiO₂, which is a well-known UV-sensible reference
106 photocatalyst offering a weak absorbance in acid media. Because of this, this
107 activity concerned participation of intraband defect levels and not to the common
108 photocatalytic mechanism involving the interband electronic transitions. Many
109 points, including the component mass ratio and type of binding between the
110 constituting organic and inorganic components have to be explored in order to
111 understand potentiality of the TiO₂-cellulose nanocomposites in photocatalysis.
112 In this work, we developed a method for synthesis of a composite material,
113 consisting of TiO₂ nanoparticles strongly bound to microcrystalline cellulose and
114 possessing an enhanced photocatalytic activity owing to a specific participation of
115 both constituting components.

116 **Experimental**

117 Caproic acid (Aldrich, 98%), n-decane (Aldrich, 99%), titanium tetraisopropoxide
118 (TTIP, Aldrich, 97%) and microcrystalline cellulose (MCC, Aldrich, 10 wt. %
119 H₂O) were used in the synthesis. Caproic acid and n-decane were additionally
120 dried over molecular sieves (Merck). To obtain anhydrous cellulose if necessary,
121 the commercial MCC was dried at 110°C in a vacuum (0.1 mm Hg). All
122 manipulations preceding the heat treatment in an autoclave were performed in a
123 glove box filled with dry argon.

124 In a typical experiment, TTIP was dissolved in 15 mL of caproic acid (or in 15
125 mL of n-decane), and 1 g of MCC was added. After a thorough mixing, the
126 reaction mixture was placed in a Teflon liner of a steel autoclave (internal volume
127 50 mL) under argon and heated to 200°C. The samples were separated on a Schott
128 filter, washed successively with decane, petroleum ether, and alcohol and dried
129 thereafter without any contact with atmospheric moisture.

130 The samples were examined by IR spectroscopy (FSM-2201 device) and X-ray
131 diffraction (Rigaku SmartLab 3 diffractometer, CuK_α radiation, $\lambda = 1.54051$ Å)
132 methods. The particle crystalline size was determined from the (101) diffraction

133 line width using the Scherrer equation. The crystallinity index (CrI) was
134 calculated as the ratio of the highest peak (crystalline peak I_{200}) to that of the
135 minimum (I_{am}) (Segal et al. 1959) between the (110) and (102)/(012) peaks at
136 about $2\theta = 18.5^\circ$ (French 2014). Examination of each of the sample (MCC,
137 TiC(1-4)) results in curves whose measured heights above a base line at $2\theta =$
138 18.5° and 22.8° gave the value I_{am} and I_{200} respectively.

$$139 \quad CrI = \frac{I_{200} - I_{am}}{I_{200}}$$

140 The specific surface area was estimated by the BET method, pore volume, and
141 average pore size were estimated by the BJH method from the nitrogen
142 adsorption/desorption isotherms measured with Quantachrome NOVA 1200e
143 instrument. For measurements samples were treated at 110°C in vacuum (<0.1
144 mmHg) for 2 h. The transmission electron micrographs (TEM) were taken with a
145 JEOL JEM-100C device, after preparing the analytic samples in chloroform. ^1H
146 NMR spectra were recorded with JEOL ECX-400A instrument at 400 MHz, after
147 preparing the analytic samples in benzene- d_6 . The UV-visible absorption spectra
148 of the samples prepared were measured with SF-2000 spectrometer equipped with
149 an integrating sphere. The thermal analysis was performed with Netzsch STA 429
150 device under dry argon gas atmosphere.

151 The photocatalytic activity of the materials prepared was evaluated by monitoring
152 the decomposition of formic acid ($pK_a = 3.75$, initial concentration 0.35 mmol/l)
153 in aqueous solution of a total volume 100 mL. Prior to UVA irradiation, every
154 synthesized sample of 10 mg mass was dispersed during 10 min under ultrasound
155 in 1 mL of water until a stable suspension of was formed. When using caproic
156 acid, 1% KOH solution was taken instead of water, with the subsequent
157 neutralization to pH 5. The photocatalytic medium was prepared under air flow in
158 a dark under magnetic stirring for 30 min. The prepared suspensions were
159 irradiated with a DRL-100 high-pressure mercury lamp under continuous
160 magnetic stirring. The lamp emits in the UV-visible range with the most intense
161 UVA line at ~ 365 nm (90% of the lamp intensity). The reaction solutions were
162 periodically analyzed, and the initial (C_0 , $t=0$) and current (C , $t>0$) formic acid
163 concentrations were calculated from the solution acidity. The solution acidity was
164 determined with an I-510 ionometric converter with an accuracy of ± 0.01 pH unit.
165 Aeroxide P25 TiO_2 (Sigma-Aldrich) of a mean particle size 21 nm and specific
166 surface area 35-65 m^2/g (BET) was used as a reference sample.

167 To evaluate the effect of the mass exchange on the rate of photocatalytic
 168 decomposition of formic acid, the stirring rate of the photocatalytic medium was
 169 varied from 200 to 800 rpm. These measurements revealed no appreciable
 170 influence of stirring on the decomposition rate, which permits to conclude that the
 171 mass transport was not a limiting stage in our experimental conditions and that the
 172 decomposition rate depends mostly on the material activity.

173 A list of the synthesized samples along with their preparation conditions are
 174 summarized in Table 1. Samples indicated as TiD and TiC were respectively
 175 prepared in decane and in caproic acid and samples TiDH₂O and TiO₂D₂ were
 176 prepared in decane from commercial cellulose. The synthesis of all samples was
 177 performed at 200°C. The details of preparation given in Table 1.

178 **Table 1.** Synthesis conditions and photocatalytic rate constant (R) of TiO₂-MCC composites.

Sample	Solvent	Reaction time (h)	TiO ₂ content (g)**	R (h ⁻¹)***	Error bars +/-
TiDH ₂ O	n-decane	8	0.27	0.100	0.005
TiD1	n-decane	8	0.27	0.153	0.006
TiD2	n-decane	15	0.27	0.195	0.008
TiD3	n-decane	30	0.27	0.223	0.008
TiO ₂ D ₂ *	n-decane	15	0.27	0.273	0.017
TiC1	caproic acid	8	0.05	0.278	0.011
TiC2	caproic acid	8	0.13	0.520	0.020
TiC3	caproic acid	8	0.27	0.600	0.033
TiC4	caproic acid	8	0.54	0.654	0.036
TiC5	caproic acid	2	0.27	0.408	0.011
TiC6	caproic acid	4	0.27	0.458	0.012
TiO ₂ C ₃ *	caproic acid	8	0.27	0.343	0.010
TiO ₂ P25				0.732	0.040

179 * Samples prepared with an additional calcination at 500°C for 2 h.

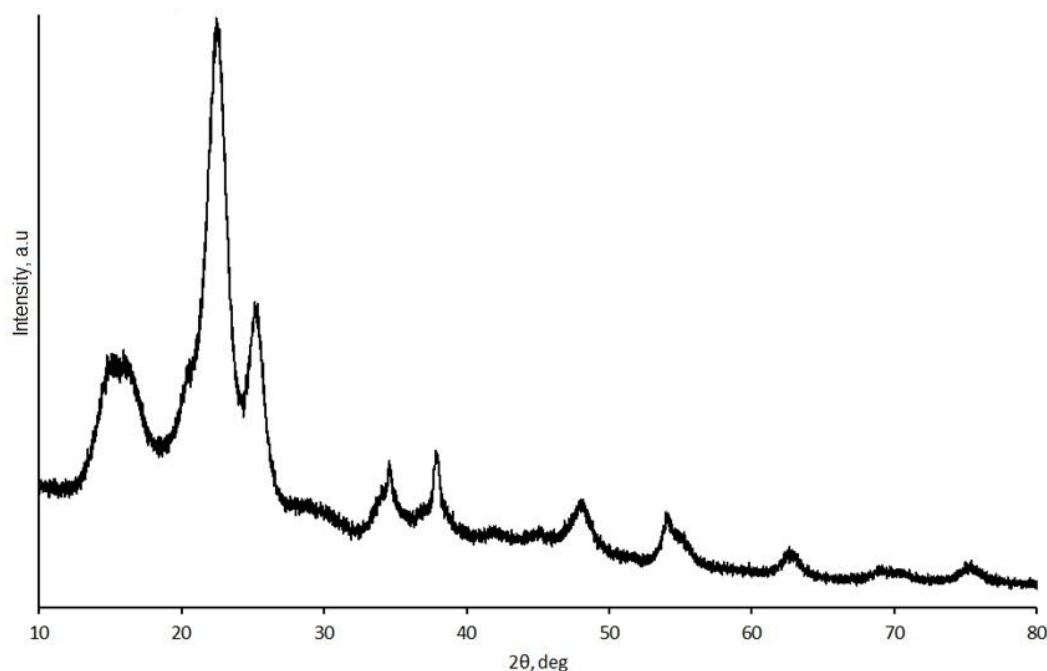
180 ** TiO₂ content corresponds to the initial TTIP amount mixed with 1 g MCC.

181 *** Corresponds to the first order kinetics. Tests were performed with 10 mg powders.

182

183 Results and Discussion

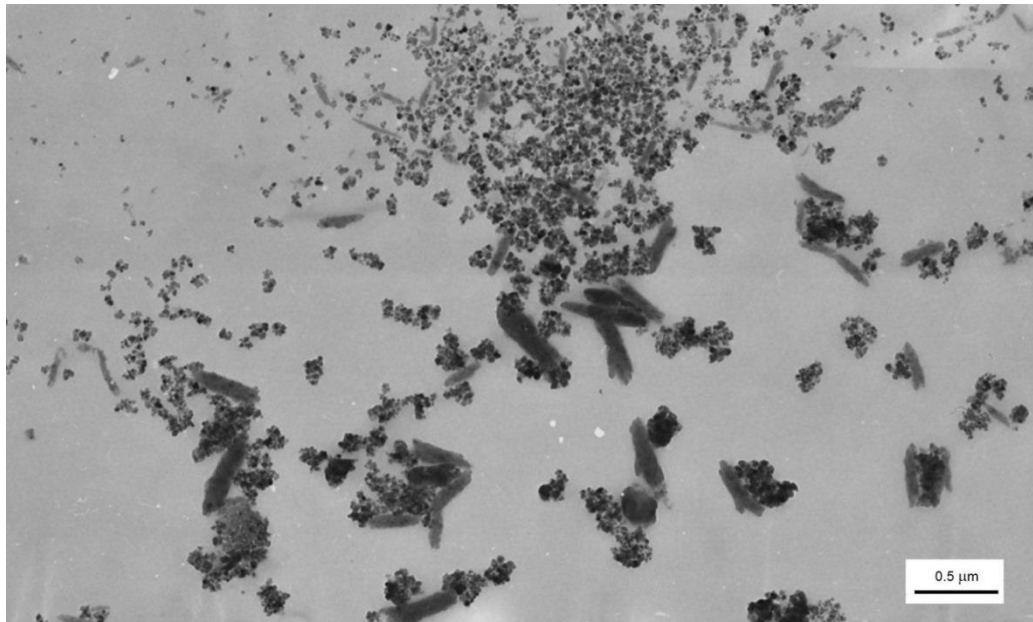
184 Our attempts failed to prepare anatase TiO_2 -MCC composites using the
185 commercial MCC. This is apparently due to the fact that hygroscopic cellulose
186 contains about 10 wt% of water. The X-ray diffraction analysis of TiDH_2O
187 sample (Fig. 1) showed that nanosized anatase is formed when performing the
188 synthesis in TTIP-MCC (commercial)-*n*-decane system but anatase and MCC
189 behave as the independent components. In fact, TEM micrograph in Fig. 2 clearly
190 shows that majority of anatase TiO_2 crystallites were separated from MCC grains,
191 forming a mixture of a priori non-interacting particles (TiDH_2O). An increase in
192 the cellulose grain size may be attributed to a partial grains sintering. In this case,
193 one cannot expect any synergy revealed by the material components in the
194 photocatalytic process.



195

196 **Figure 1.** X-ray diffraction data of TiDH_2O sample.

197

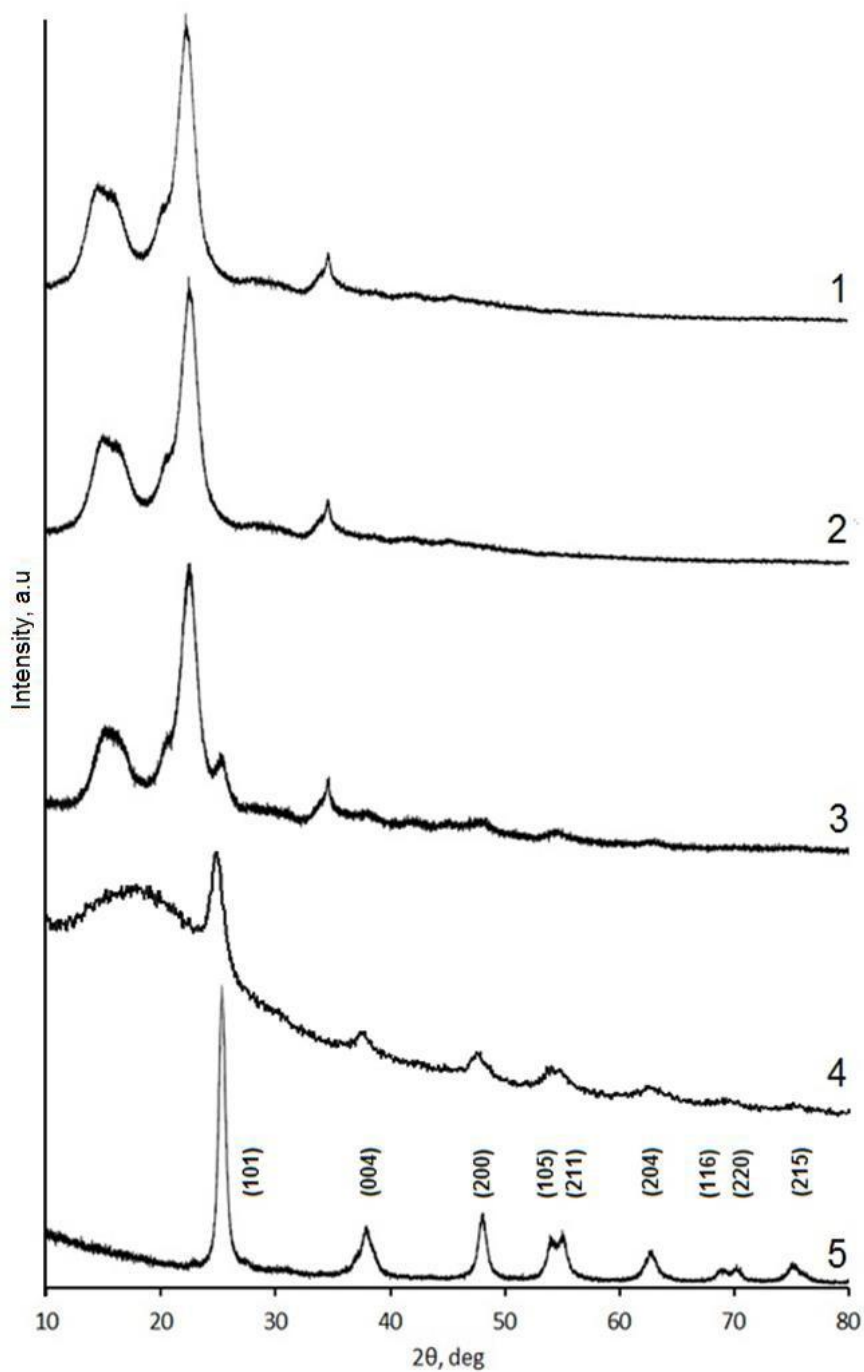


198

199 **Figure 2.** TEM micrograph of TiDH₂O sample.

200

201 The reaction of TTIP with anhydrous MCC in n-decane is rather slow, as
202 confirmed by the fact that Bragg reflections of anatase TiO₂ did not significantly
203 show up in X-ray diffraction pattern of TiD1 sample (Fig. 3), even after 8 hours of
204 the reaction runtime, which pattern is almost identical to that of pure cellulose
205 (MCC).

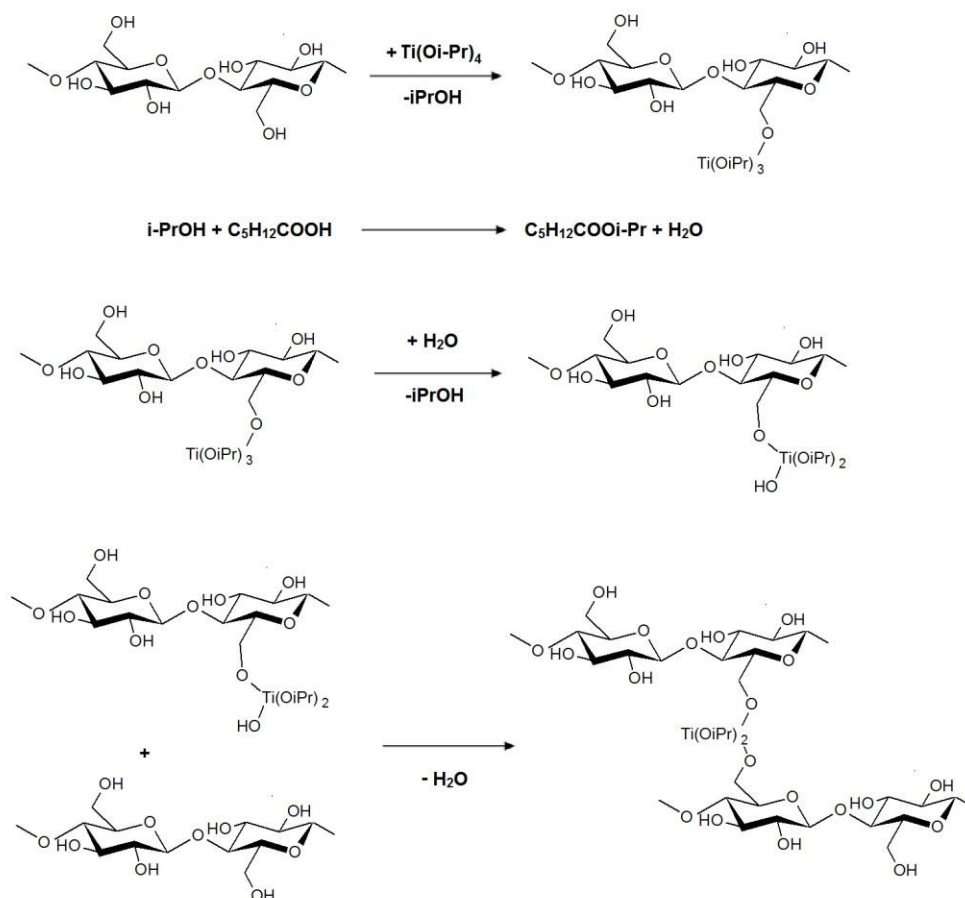


206

207 **Figure 3.** X-ray diffraction data of MCC (1), TiD1 (2), TiD2 (3), TiD3 (4) and TiO₂D2 (5).

208

209 The titania attachment to the cellulose surface begins in these conditions through
 210 the condensation reactions between the most active hydroxy group of cellulose at
 211 C⁶ carbon atom and OR- of Ti cation with the release of isopropyl alcohol (Fig. 4).



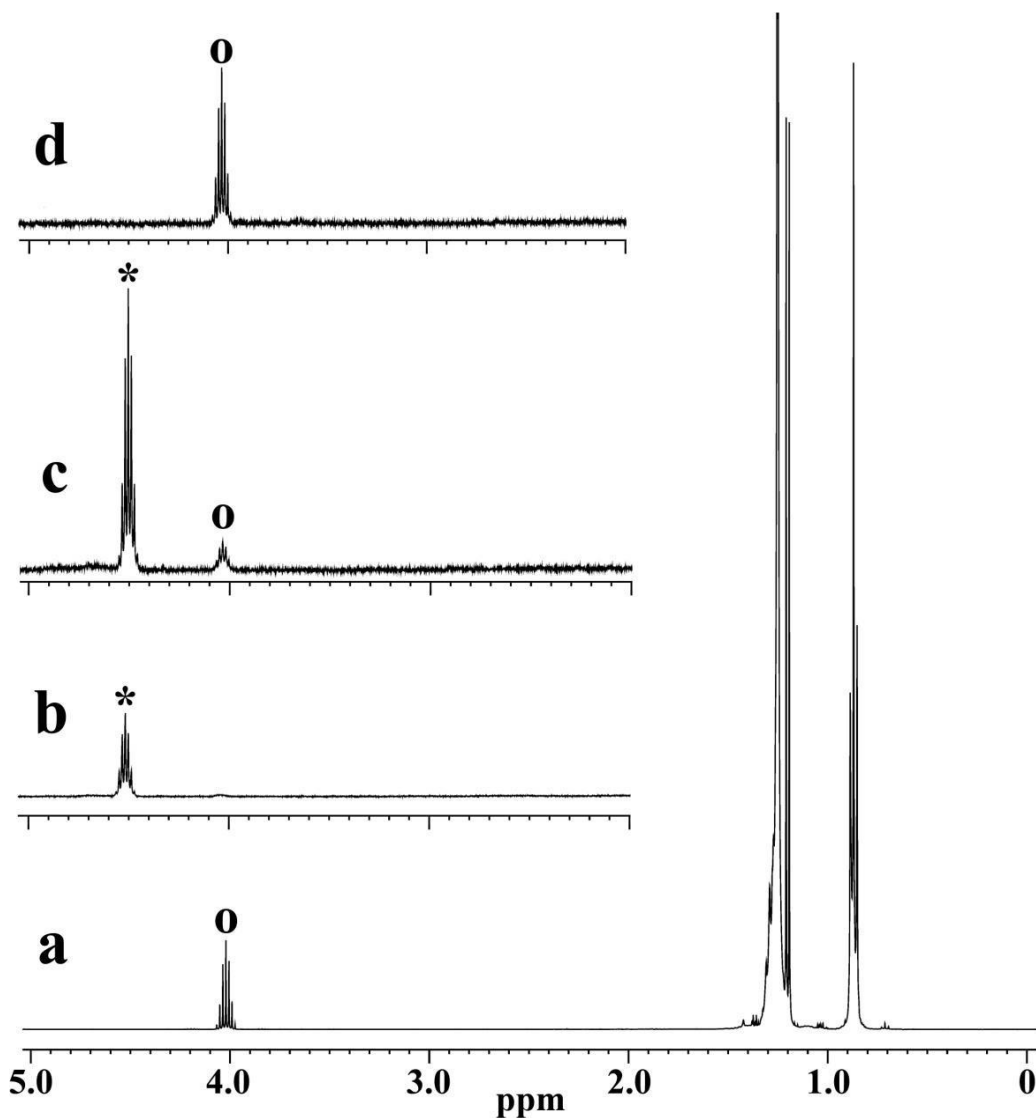
212

213 **Figure 4.** Tentative reaction scheme.

214

215 This process was confirmed by ^1H NMR measurements shown in Fig. 5. Two
 216 solutions of TTIP and isopropyl alcohol in decane and reference samples were
 217 examined in this series. The signal of the decane proton was observed in all
 218 spectra at high fields ($\delta < 1.5$ m.d). The proton of the secondary carbon atom in
 219 TTIP gives a septet at 4.50 ppm ($J = 6.18$ Hz), and the relevant proton in
 220 isopropyl alcohol molecule gives a septet at 4.03 ppm ($J = 6.11$). The
 221 solvothermal process leads to smearing of the septet, suggesting distortion
 222 symmetry of the substituents at the titanium atom when isopropyl alcohol appears.
 223 We notice that the control series performed without TTIP showed that MCC was
 224 stable in the experimental conditions with the weight loss of the material below
 225 0.2% during 8 hours of the autoclave treatment. A noticeable amount of anatase
 226 TiO_2 was only obtained after a heat treatment of the reaction mixture in the
 227 autoclave for a longer time (TiD2 and TiD3 samples) and/or higher temperature
 228 (TiO_2D_2 sample), as show X-ray diffraction patterns of in Fig. 3. However,
 229 cellulose underwent a gradual degradation in this case; this can be seen from

230 comparison of curves 2, 3 and 4, where reflexes of MCC continuously weakened
231 and disappeared.

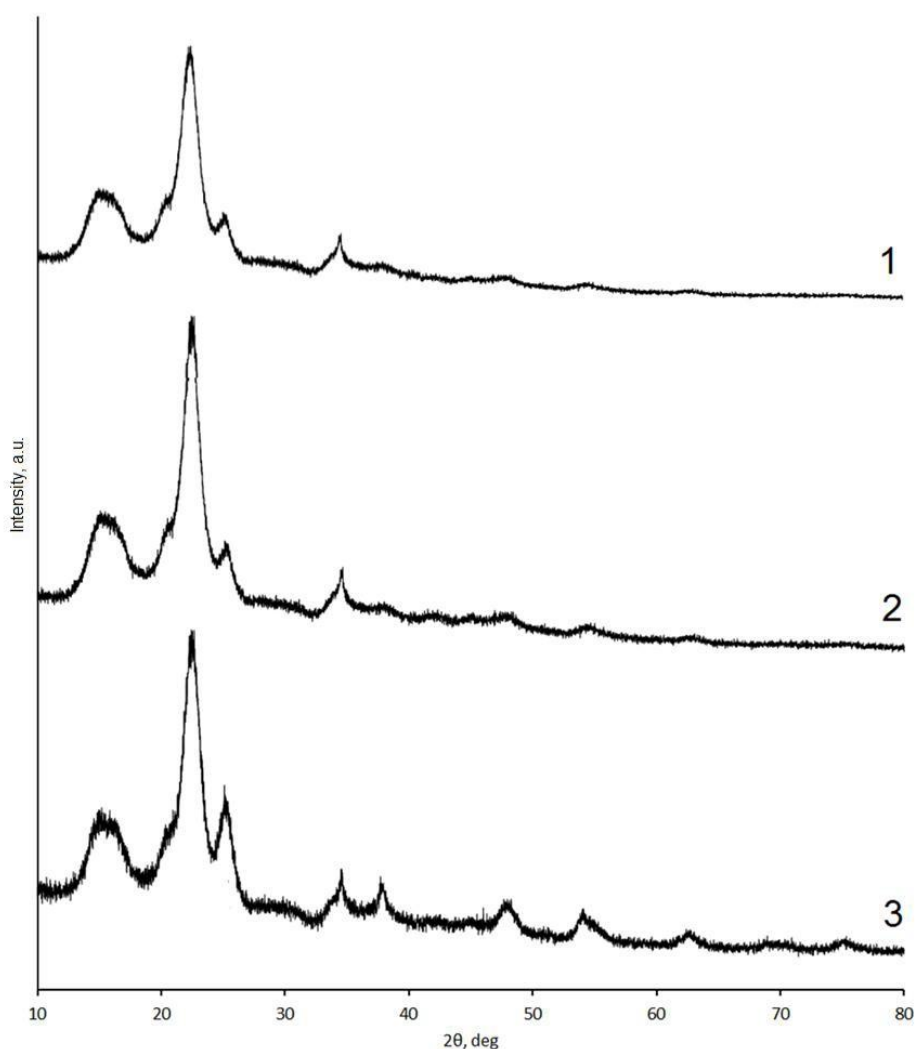


232

233 **Figure 5.** ¹H NMR spectra of isopropyl alcohol in decane (a), TTIP in decane (b), reaction mixture
234 after 2 h (c), reaction mixture after 8 h (d).

235

236 In order to obtain a stable anatase TiO₂-MCC composite, n-decane solvent, which
237 did not work, was replaced by caproic acid contributed to the synthesis as reagent
238 and solvent in the same time. In the caproic acid medium, water is released in situ,
239 and this fact allows the composite formation process to be controlled. This
240 mechanism has been previously studied in Ref. [Zdravkov et al. 2015]. Fig. 6
241 shows that the formation of the anatase structure occurs already in the first 2 hours
242 of the reaction and the formation of anatase TiO₂-MCC composite was completed
243 after 8 hours.



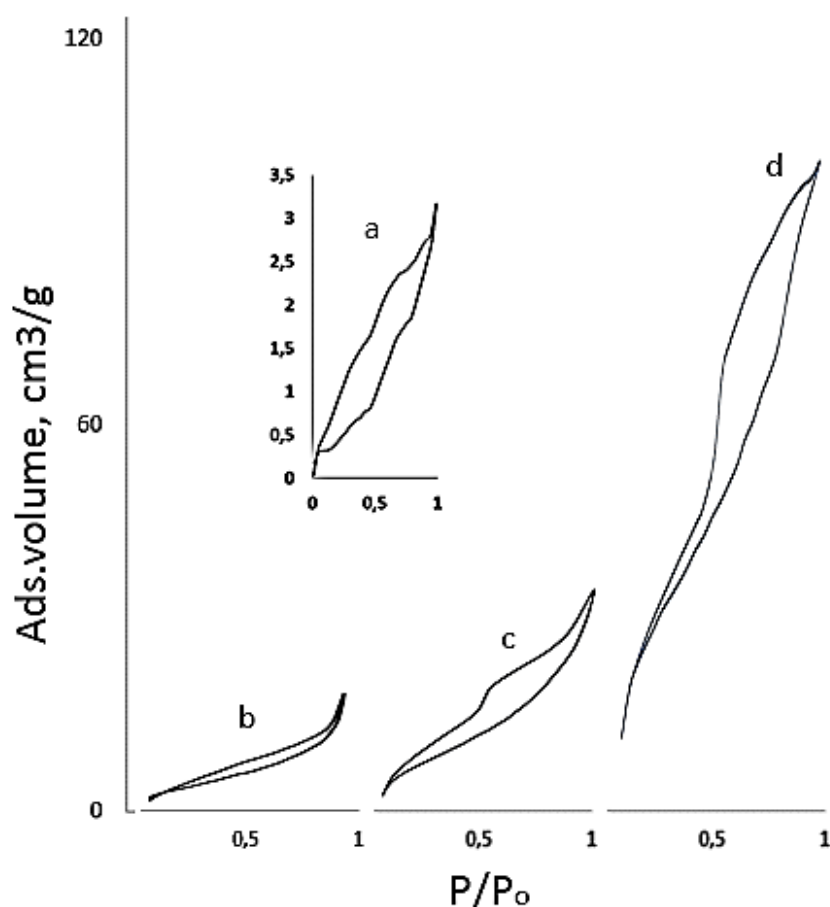
244

245 **Figure 6.** X-ray diffraction data of TiC5 (1), TiC6 (2), TiC3 (3).

246

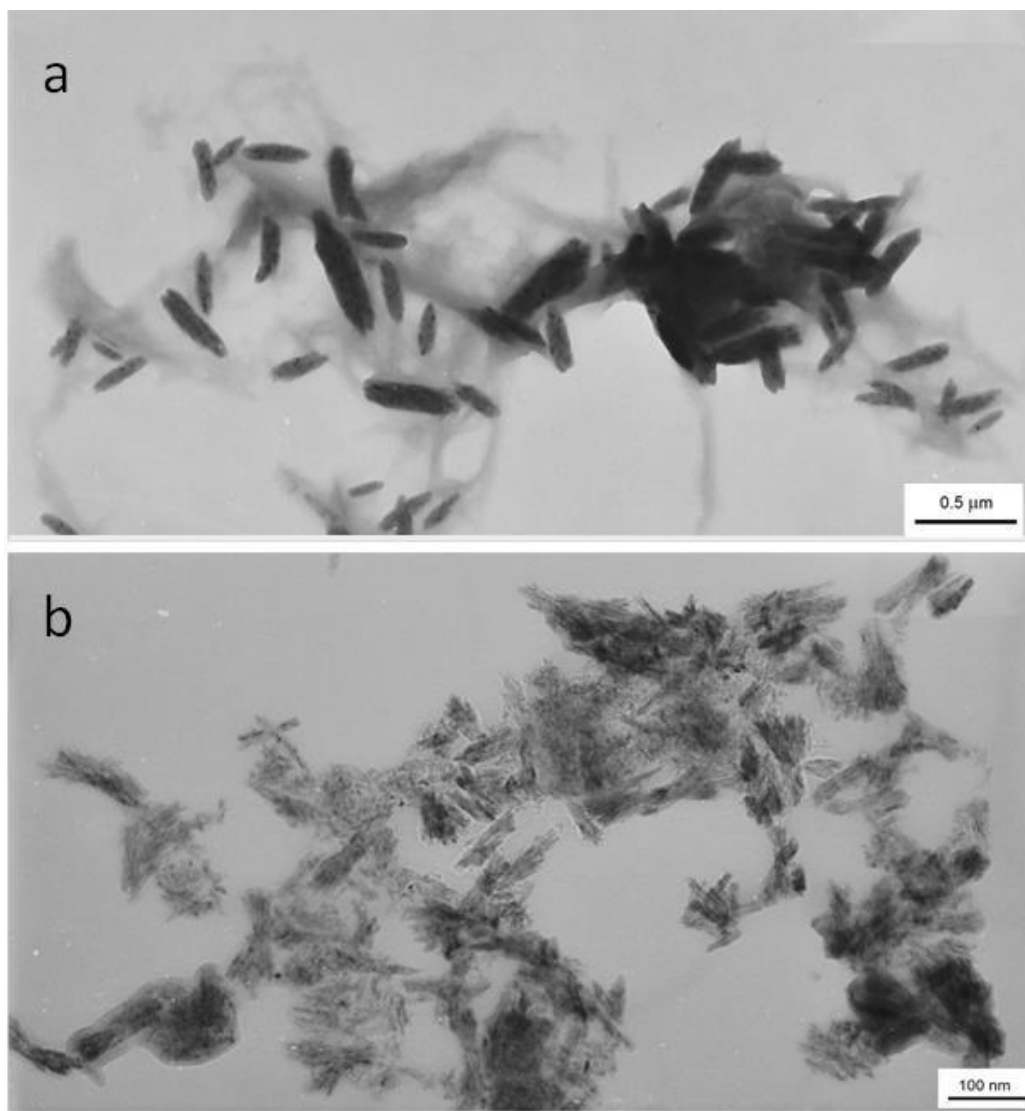
247 According to TEM images in Fig. 8, the synthesis is accompanied by loosening of
 248 MCC grains in course of the anatase immobilization. This process is accompanied
 249 by a partial cellulose degradation, which was confirmed by nitrogen
 250 sorption/desorption data. The surface area, pore volume, and pore diameter of TiC
 251 samples with different titania contents and those of the reference Aeroxide P25
 252 TiO₂ are summarized in Table 2. These parameters suggest high adsorption
 253 activity of samples TiC1, TiC3, and, especially, TiC4. The isotherms evaluated
 254 for MCC-TiO₂ composites were classed with type IV and V isotherms, suggesting
 255 the micro- and mesoporous character of the samples. For sample TiC4, the
 256 amount of nitrogen adsorbed rapidly increases at all relative pressures, reaching
 257 95 cm³/g (Fig. 7d). The pore size distribution for sample TiC4 has a single narrow
 258 peak indicating that this sample is highly homogeneous.

259 Isotherms and pore radius distributions for samples TiC1 and TiC3 have the
 260 similar shape, but the amount of adsorbed nitrogen is different [for TiC1, the
 261 amount is 20 cm³/g (Fig. 7b), and for TiC3, the amount is 40 cm³/g (Fig. 7c)]. For
 262 initial MCC the amount of nitrogen adsorbed is comparatively low – near 3 cm³/g,
 263 and pore size distribution was wide with several different predominant pore sizes
 264 (See Figure S8. Supporting Information). As one can see in the course of
 265 synthesis the pore size distribution became narrow. It supported the assumption,
 266 that reaction of cellulose and titanium isopropoxide goes especially at amorphous
 267 regions.



268
 269 **Figure 7.** N₂ adsorption/desorption isotherms for MCC (a), TiC1 (b), TiC2 (c), and
 270 TiC4 (d).

271
 272 The specific surface area of TC samples proportionally increases with the increase
 273 of titania content, which is characteristic of particles undergoing insignificant
 274 coarsening. The mean size of TC series crystalline particles, calculated by
 275 Scherrer equation from curves 3 and 4 (Fig. 3) and curve 3 (Fig. 6) was about 30
 276 nm.



277

278 **Figure 8.** TEM micrographs of MCC (a) and TiC4 (b) samples.

279 At the same time, during the formation of MCC-TiO₂ composite, the degree of
280 crystallinity of cellulose increases from 91% (pure MCC) to 98% (TiC4) with an
281 increase in the concentration of titanium dioxide. This can be explained by the
282 fact that the reaction between the components (Equations 1-4) proceeds primarily
283 through the most accessible and active groups located in the amorphous regions.
284 The data on crystallinity of cellulose were obtained by Segal method [Segal et al.
285 1959; Yacenko et al. 2019]. For more details, see Supporting Information.

286

287

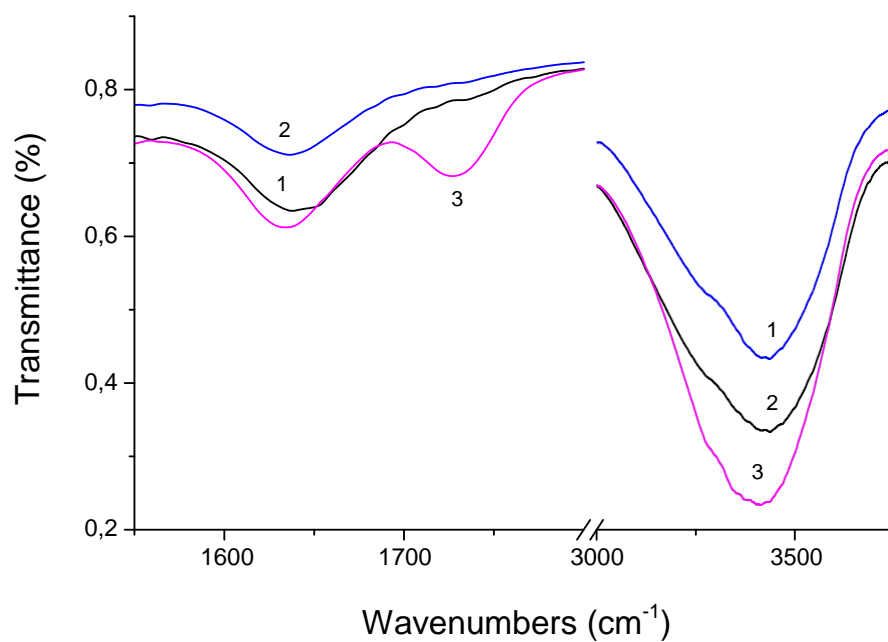
288

289

290 **Table 2.** Area, average pore radius and pore volume of samples with different titania content
 291 (TiC1, TiC2, TiC3, TiC4) and Aeroxide P25 TiO₂.

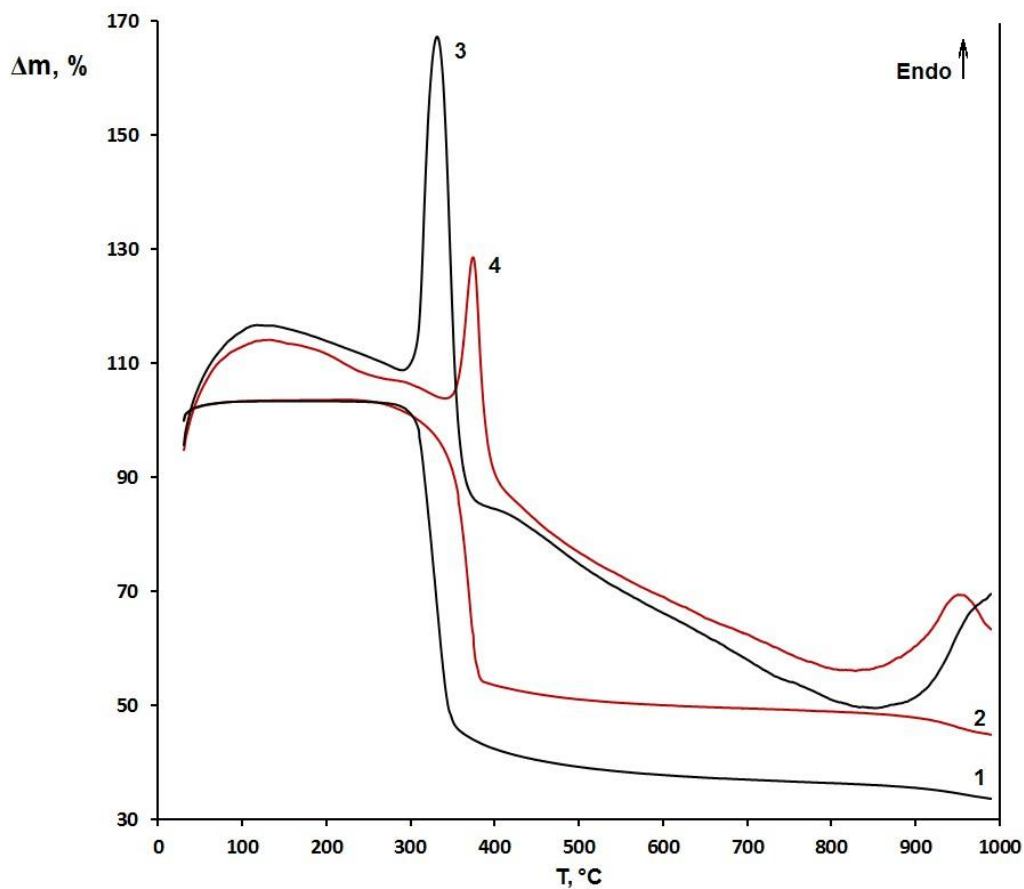
Sample	Specific surface area, m ² /g	Average pore diameter, Å	Pore volume, cm ³ /g
MCC	2.5	21	0.004
TiC1	10.2	<16	0.018
TiC3	27.4	17.7	0.037
TiC4	55.0	19.5	0.060
Aeroxide P25 TiO ₂	50.9	16	0.12

292
 293 The formation of anatase TiO₂-MCC composites was also confirmed by FTIR
 294 spectroscopy and thermal analysis. An example of pure cellulose MCC and
 295 composite TiC4 sample with the highest titania content (see Table 1) is given in
 296 Fig 9. The strong IR band of hydroxyl bending vibrations in cellulose at 1630
 297 cm⁻¹ was observed to shift to lower frequencies upon the composite formation,
 298 down to 1620 cm⁻¹ in TiC4, suggesting strong interfacial interaction between
 299 hydroxy groups of MCC and cations of titania nanoparticles. In the case of TiD
 300 sample this shift in IR spectrum was not observed. The same conclusion can be
 301 drawn from the shift of the stretching vibration band of cellulose hydroxyls at
 302 3430 cm⁻¹ to lower frequencies: 3410 cm⁻¹ in the composite material (Fig. 9). The
 303 TG-DSC analysis indicated a progressive decomposition of cellulose with an
 304 increase of temperature, accompanied by a release of different gaseous products
 305 including hydrogen, methane, carbon monoxide, etc. The thermolysis process in
 306 argon atmosphere is characterized by endothermic peaks of DSC curves. The
 307 results in Fig. 10 show that the main endothermic peak of MCC was shifted to
 308 higher temperatures by 42 °C in TiC4 composite while its magnitude was
 309 decreased from 1.32 mW/mg to 0.57 mW/mg. This confirms a tight coupling
 310 between the two components of the composite. The ~50% weight loss in the
 311 temperature range of thermolysis, observed in TiC4 compared with MCC,
 312 validates the presence of stable inorganics.



313

314 **Figure 9.** IR spectra of MCC (1), TiD1 (2) and TiC4 (3) samples.

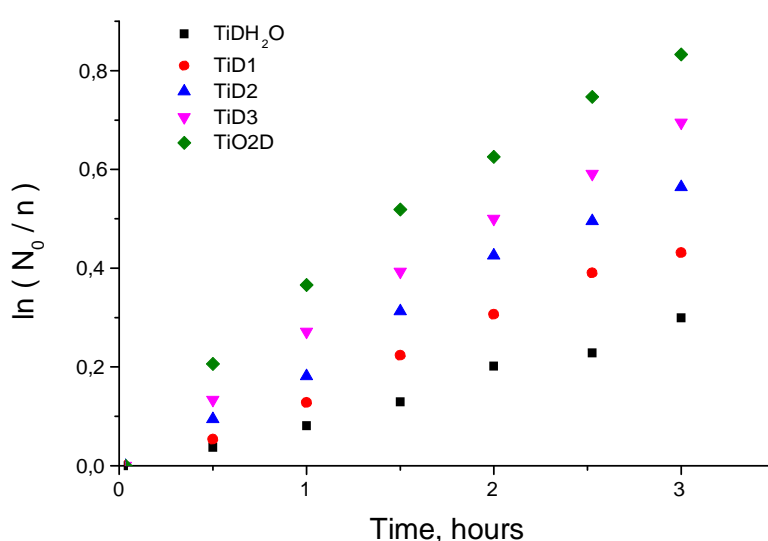


315

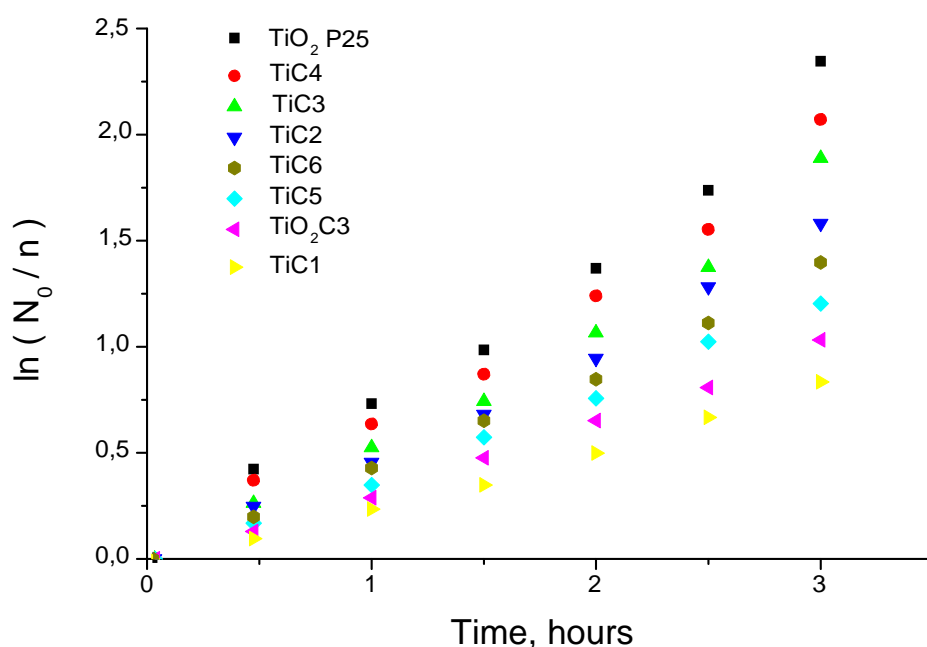
316 **Figure 10.** TG (1, 2) and DSC (3, 4) analyses of MCC (1, 3) and TiC4 (2, 4) samples under argon
 317 atmosphere.

318

319 In the photocatalytic experiments, formic acid was used as a model pollutant not
 320 sensitive to UVA radiation, which favorably distinguishes it from commonly used
 321 dyes rhodamine and methylene blue. The kinetics of the formic acid degradation
 322 is shown in Figs 12 and 13 in a semi-logarithmic frame, which evidences the first
 323 order decomposition kinetics, far from saturation phenomena. The photocatalytic
 324 rate constants in Table 1 were obtained from the linear least-squared fits of the
 325 experimental data. The kinetics observed with TD samples was relatively slow
 326 (Fig. 11). The thermal post-treatment (TiO₂D sample) did not significantly
 327 enhance the material activity, which remained much slower compared to that of
 328 commercial TiO₂ P25 photocatalysts. This correlates with our XRD measurements
 329 shown poor crystallization of anatase TiO₂ in the n-decane synthesis conditions.
 330 In contrast, TC samples synthesized in caproic acid exhibited an appreciably faster
 331 kinetics (Fig. 12) corresponding to their higher photocatalytic activity; among
 332 these samples, TiC4 prepared with the highest titania content possessed the highest
 333 activity. We notice that because of a steric factor, the hydroxy group at C-
 334 6 carbon atom of cellulose is expected to be most active in the titania attraction.
 335 Because of this, the effective amount of anatase in the composite material cannot
 336 exceed a limit imposed by the cellulose content, which is expected to be about 50
 337 wt%. Apparently, this limit is attained in TiC4 sample and further increase of the
 338 titania content is inappropriate.



339
 340 **Figure 11.** Kinetics of formic acid decomposition under UV irradiation in aqueous solutions using
 341 TiDH₂O, TiD1, TiD2, TiD3 and TiO₂D photocatalysts.



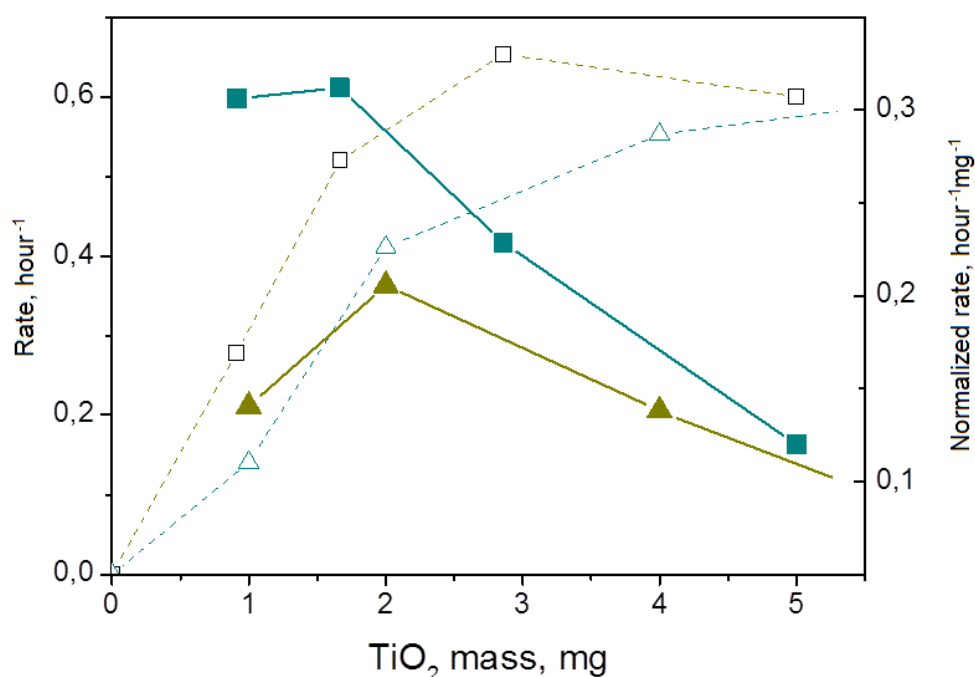
342

343 **Figure 12.** Kinetics of formic acid decomposition under UV irradiation in aqueous solutions using
 344 TiC1, TiC2, TiC3, TiC4, TiC5, TiC6, TiO₂C3 and TiO₂ P25 photocatalysts.

345

346 A deeper comparison between our best prepared and reference TiO₂ P25
 347 photocatalysts can be performed based on the intrinsic efficiency γ defined as the
 348 conversion yield of an absorbed photon to a chemical reaction. This is an
 349 important characteristic showing potentiality of the material application in the
 350 photocatalytic process. It can be shown that for a relatively small mass and first
 351 order process kinetics, γ is proportional to the reaction rate constant R normalized
 352 on the photocatalyst mass [Cheng et al. 2018; Bouslama et al. 2012]. This
 353 normalized rate reflects the material effectiveness when the photocatalyst mass is
 354 relatively small and decreases at the larger masses due to the saturation of light
 355 absorbance in accordance with the Beer-Lambert law. Our first order kinetics
 356 permits this comparison of the material activities. Fig. 12 shows reaction rates and
 357 normalized reaction rates of the best composite materials of TiC series in
 358 comparison with the reference TiO₂ P25. These rates, reported in Table 1, were
 359 obtained from the slopes of the experimental data presented in semi-logarithmic
 360 frame of $\ln(C_0/C)$ versus time of UVA illumination. As expected, the
 361 decomposition rate increases with an increase of the photocatalyst mass in both
 362 TC and TiO₂ P25 materials because of an increased light absorbance, and
 363 saturates when UVA lamp power is totally absorbed by the material. The

364 saturation rates of both types of materials were found similar. Similarly, both TC
 365 and TiO₂ P25 materials reached the maximal normalized rates (on photocatalyst
 366 mass) at the same TiO₂ loadings, apparently indicating similar effectiveness in
 367 screening the UVA lamp photons related to the morphology factors (specific
 368 surface area and particle size of titania component). However, values of the
 369 maximum normalized rates were different and that of TC photocatalysts was
 370 almost two times higher compared to TiO₂ P25. The higher intrinsic efficiency (γ)
 371 of TC composites could not be an explanation, since absolute rates at infinite
 372 photocatalyst mass of TC and reference materials were similar (Fig. 13). In
 373 contrast, finer granulometry of TC composite particles could be a reason. Indeed
 374 large agglomerates of TiO₂ P25 particles (practically of size above 100 nm)
 375 possess a significant screened volume, not accessible by UV lamp photons; as a
 376 result, this material has a significant mass, which is excluded from the
 377 photocatalytic process. In contrast, the TC component, which strongly scatter and
 378 not absorbed UVA light [Lu et al. 2013], effectively increase the residence time of
 379 UVA photons in the reaction volume; the longer interaction time creates
 380 conditions for a more efficient light energy deposition into the photocatalyst.



381

382 **Figure 13.** Absolute (□; ▲) and normalized on photocatalyst mass (■; ▲) decomposition rates of
 383 formic acid observed with TC (□, ■) and TiO₂ P25 (▲, ▲) photocatalysts.

383

384 **Conclusion**

385 In this work, novel cellulose-TiO₂ composite photocatalysts were synthesized via
386 solvothermal method in order to assemble microcrystalline organic cellulose and
387 inorganic titania components. Two series of materials were prepared in n-decane
388 and caproic acid solvents. In n-decane, the synthesis resulted in a poor
389 crystallization of anatase titania and the subsequent thermal post treatment
390 destroyed the composites. In contrast, in caproic acid, acting as solvent and
391 reagent, anatase TiO₂ nanoparticles were formed onto the crystalline domains of
392 cellulose. Strong covalent bonds between the organic and inorganic components
393 of the composite were evidenced by IR spectroscopy, ¹H NMR and TG/DSC
394 methods. The photocatalytic activity of the synthesized materials was evaluated by
395 the decomposition of formic acid in aqueous solutions under UVA lamp
396 illumination and compared with that of reference photocatalyst Aeroxide P25
397 TiO₂. The absolute activities of composites and reference photocatalyst were
398 similar. On the other hand, much smaller titania mass was required in order to
399 reach the maximum activity in the prepared composites compared to the reference
400 photocatalyst. This effect was attributed to the organic component, which
401 effectively scatters UVA lamp photons, thus increasing efficiency of the light
402 energy deposition into the inorganic anatase TiO₂ component.

403 **Acknowledgments.** Authors are grateful to Ministry of Science and Higher Education of Russian
404 Federation for financial support (Project No 0097-2019-0017).

405 **References**

- 406 Bouslama M, Amamra MC, Jia Z, Ben Amar M, Brinza O, Chhor K, Abderrabba M, Vignes
407 JL, Kanaev A (2012) Nanoparticulate TiO₂-Al₂O₃ photocatalytic media: effect of particle size and
408 polymorphism on photocatalytic activity. ACS Catal 2:1884-1892; doi:10.1021/cs300033y
- 409 Brandes R, Souza L, Vargas V, Oliveira E, Mikowski A, Carminatti C, Al-Qureshi H,
410 Recouvreux D (2016) Preparation and Characterization of Bacterial Cellulose/TiO₂ Hydrogel
411 Nanocomposite. Journal of Nano Research 43:73-80;
412 doi:10.4028/www.scientific.net/JNanoR.43.73
- 413 Butman MF, Ovchinnikov NL, Karasev NS, Kochkina NE, Agafonov AV, Vinogradov AV
414 (2018) Photocatalytic and adsorption properties of TiO₂-pillared montmorillonite obtain by
415 hydrothermally activated intercalation of titanium polyhydroxo complexes. Beilstein J.
416 Nanotechnol 9:364-378; doi:10.3762/bjnano.9.36

417 Cardoso GV, Mello LR, Zanatta P, Cava S, Raubach CW, Moreira ML (2018) Physico-
418 chemical description of titanium dioxide–cellulose nanocomposite formation by microwave
419 radiation with high thermal stability. *Cellulose* 25:2331–2341; doi:10.1007/s10570-018-1734-2
420 Cheng K, Chhor K, Passarello JP, Colbeau-Justin C, Kanaev A (2018) Photocatalytic
421 nanoparticulate $Zr_xTi_{1-x}O_2$ coatings with controlled homogeneity of elemental composition.
422 *Chemistry Select* 3:11118–11126; doi:10.1002/slct.201801732
423 Dette C, Pérez-Osorio MA, Kley CS, Punke P, Patrick CE, Jacobson P, Guistino F, Jung SJ,
424 Kern K (2014) TiO_2 anatase with a bandgap in the visible region. *Nano Lett* 12:6533–6538; doi:
425 10.1021/nl503131s
426 Farag S, Amr A, El-Shafei A, Ibrahim HM, Asker MS (2017) Influence of bacterial cellulose
427 for synthesis and application of titanium dioxide nanoparticles compared with sol-gel method.
428 Proceedings of 60th The IRES International Conference, Munich, Germany 15-23
429 Filippo E, Carlucci C, Capodilupo AL, Perulli P, Conciauro F, Corrente GA, Gigli G,
430 Ciccarella G (2015) Enhanced photocatalytic activity of pure anatase TiO_2 and Pt- TiO_2
431 nanoparticles synthesized by green microwave assistant route. *Mater. Res* 18:473;
432 doi:10.1590/1516-1439.301914
433 French AD (2014) Idealized powder diffraction patterns for cellulose polymorphs. *Cellulose*
434 21:885-896; doi: 10.1007/s10570-013-0030-4
435 Galkina OL, Sycheva A, Blagodatskiy A, Kaptay G, Katanaev VL, Seisenbaeva GA, Kessler
436 VG, Agafonov AV (2014) The sol-gel synthesis of cotton/ TiO_2 composites and their antibacterial
437 properties. *Surface & Coatings Technology* 253:171–179; doi:10.1016/j.surfcoat.2014.05.033
438 Garusinghe UM, Raghuwanshi VS, Batchelor W, Garnier G (2018) Water resistant cellulose-
439 titanium dioxide composites for photocatalysis. *Sci Rep* 8:2306; doi:10.1038/s41598-018-20569-w
440 Gorbovyi P, Uklein A, Tieng S, Traore M, Chhor K, Museur L, Kanaev A (2011) Novel
441 nanostructured pHEMA-(oxo) TiO_2 hybrid materials with efficient light-induced charge separation,
442 *Nanoscale* 3:1807–1812; doi: 10.1364/OME.3.000533
443 Habibi S, Jamshidi M (2020) Synthesis of TiO_2 nanoparticles coated on cellulose nanofibers
444 with different morphologies: Effect of the template and sol-gel parameters. *Mater. Sci. in*
445 *Semiconductor Processing* 109:104927; doi:10.1016/j.mssp.2020.104927
446 He D, Li Y, Wang J, An Q (2016) Tunable nanostructure of TiO_2 reduced oxide composite for
447 high photocatalysis. *Applied Microscopy* 46:37–44; doi:10.9729/AM.2016.46.1.37
448 Ioelovich M. (2014) *Cellulose: Nanostructured natural polymer*. Saarbrücken: Lap Lamber
449 Acad, 100.
450 Kaseem M, Hamad K, Rehman ZU (2019) Review of Recent Advances in Poly(lactic
451 Acid/ TiO_2 Composites. *Materials* 12:3659; doi:10.3390/ma12223659
452 Kayaalp M, Rathousk J, Bein T (2014) Tailoring the morphology of mesoporous titania thin
453 film through biotemplating with nanocrystalline cellulose. *J. Am. Chem. Soc* 136:5930–5937;
454 doi:10.1021/ja411292u
455 Khalid A, Ullah H, Ul-Islam M, Khan R, Khan S, Ahmad F, Khal T, Wahid F (2017)
456 Bacterial cellulose– TiO_2 nanocomposites promote healing and tissue regeneration in burn mice
457 model. *RSC Adv* 7:47662–47668; doi:10.1039/c7ra06699f

458 Kuznetsov AI, Kameneva O, Bitururin N, Rozes L, Sanchez C, Kanaev A. (2009) Light-
459 induced photopatterning of organic-inorganic TiO₂ based hybrid materials with tunable interfacial
460 electron transfer, *Phys. Chem. Chem. Phys* 11:1248–1257; doi: 10.1039/B814494J

461 Li Y, Zhang JC, Kong F, Li W, Yang C, Hsiao BS (2020) Facile synthesis of TiO₂/CNC
462 nanocomposites for enhanced Cr(VI) photoreduction: Synergistic roles of cellulose nanocrystals.
463 *Carbohydr. Polym* 233:115838; doi: 10.1016/j.carbpol.2020.115838

464 Lu Y, Sun Q, Liu T, Yang D, Liu Y, Li J (2013) Fabrication, characterization and
465 photocatalytic properties of millimeter-long TiO₂ fiber with nanostructures using cellulose fiber as
466 a template. *J. Alloys Compd* 577:569–574; doi:10.1016/j.jallcom.2013.06.183

467 Luo Y, Xu J, Huang J (2014) Hierarchical nanofibrous anatase-titania–cellulose composite
468 and its photocatalytic property. *CrystEngComm* 464–471; doi:10.1039/c3ce41906a

469 Melvin NHK, Leo CP (2019) The coherence between TiO₂ nanoparticles and microfibrillated
470 cellulose in thin film for enhanced dispersal and photodegradation of dye. *Progress in Organic*
471 *Coatings* 132:70–75; doi:10.1016/j.porgcoat.2019.02.017

472 Morawski AW, Kusiak-Nejman E, Przepiórski J, Kordala R, Pernak J (2013) Cellulose-TiO₂
473 nanocomposite with enhanced UV–Vis light absorption. *Cellulose* 20:1293–
474 1300; doi:10.1007/s10570-013-9906-6

475 Morshed MN, Azad SA, Deb H, Shaun BB, Shen XL (2020) Titania-loaded cellulose-based
476 functional hybrid nanomaterial for photocatalytic degradation of toxic aromatic dye in water. *J. of*
477 *Water Process Engineering* 33:101062; doi: 10.1016/j.jwpe.2019.101062

478 Mory K (2005) Photo-functionalized materials using g nanoparticles: photocatalysis. *KONA*
479 *Powder Part J* 23:205-214; doi:10.14356/kona.2005023

480 Oliveira AC, Santos MS, Brandão LMS, Resende ITF, Leo IM, Morillo ES, Yerga RMN,
481 Fierro JLG, Egues SMS, Figueiredo RT (2017) The effect of cellulose loading on the photoactivity
482 of cellulose-TiO₂ hybrids for hydrogen production under simulated sunlight. *International Journal*
483 *of Hydrogen Energy* 42:28747–28754; doi:10.1016/j.ijhydene.2017.09.022

484 Postnova I, Kozlova E, Cherepanova S, Tsybulya S, Rempel A, Shchipunov Y (2015) Titania
485 synthesized thorough regulated mineralization of cellulose and its photocatalytic activity. *RSC*
486 *Adv* 5:8544-8551; doi:10.1039/C4RA15862H

487 Rahmawati F, Fadillah M, Mudjijono I (2017) Composite of Nano-TiO₂ with Cellulose
488 Acetate Membrane from Nata de Coco (Nano-TiO₂/CA(NDC)) for Methyl Orange Degradation *J.*
489 *Mater. Environ. Sci* 8:287-297

490 Sathasivam S, Bhachu SD, Li Y, Chadwick N, Althabaiti SA, Alyobi AO, Basahel SN,
491 Carmalt CJ, Parkin IP (2015) Tungsten doped TiO₂ with enhanced photocatalytic and opt-
492 electrical properties via aerosol assisted chemical vapor deposition. *Sci. Rep* 4:10952–10956;
493 doi:10.1038/srep10952

494 Segal L, Creely JJ, Martin AE, Conrad CM (1959) An Empirical method for estimating the
495 degree of crystallinity of native cellulose using the X-ray diffractometer. *Text Res J* 29(10):786-
496 794; doi: 10.1177/004051755902901003

497 Shahrezaei M, Habibzadeh S, Babaluo AA, Hosseinkhani H, Haghighi M, Hasanzedah A,
498 Tahmasebpour R (2017) Study of synthesis parameters and photocatalytic activity of TiO₂

499 nanostructures *J. Exp. Nanosci* 12:45; doi:10.1080/17458080.2016.1258495

500 Sharon M, Modi F, Sharon M (2016) Titania based nanocomposite as a photocatalyst: A
501 review. *AIMS Materials Science* 3:1236-1254; doi:10.3934/matricsci.2016.3.1236

502 Shevtsova TA, Zlotski SV (2018) Facile sol-gel synthesis of metal oxide nanoparticles in a
503 cellulose paper template. *Doklady Bguir* 112:113–115

504 Sirvio JA, Visanko M, Heiskanen JP, Liimatainen H (2016) UV-absorbing cellulose
505 nanocrystals as functional reinforcing fillers in polymer nanocomposite films. *J. Mater. Chem. A*
506 4:6368–6375; doi:10.1039/C6TA00900J

507 Sun D, Yang J, Wang X (2010) Bacterial cellulose/TiO₂ hybrid nanofibers prepared by the
508 surface hydrolysis method with molecular precision. *Nanoscale* 2:287–292;
509 doi:10.1039/b9nr00158a

510 Tang B, Chen H, Peng H, Wang Z, Huang W (2018) Graphene Modified TiO₂ Composite
511 Photocatalysts: Mechanism, Progress and Perspective. *Nanomaterials* 8:105;
512 doi:10.3390/nano8020105

513 Tieng S, Kanaev A, Chhor K (2011) New homogeneously doped Fe(III)–TiO₂ photocatalyst
514 for gaseous pollutant degradation. *Appl. Cat. A* 399:191–197; doi:10.1016/j.apcata.2011.03.056

515 Wang SB, Pan L, Song JJ, Mi W, Zou JJ, Wang L, Zhang X (2015) Titanium-defected
516 undoped anatase TiO₂ with p-type conductivity, room-temperature ferromagnetism, and
517 remarkable photocatalytic performance. *J. Am. Chem. Soc* 137:2975–2983;
518 doi:10.1021/ja512047k

519 Wang W, Wang J, Shi X, Yu Z, Song Z, Dong L, Jiang G, Han S (2016) Synthesis of
520 Mesoporous TiO₂ Induced by NanoCellulose and Its Photocatalytic Properties. *BioResources* 11:
521 3084-3093; doi: 10.15376/biores.11.2.3084–3093

522 Wittmar A, Thierfeld H, Köcher S, Ulbricht M (2015) Routes towards catalytically active
523 TiO₂ doped porous cellulose. *RSC Adv* 5:35866–35873; doi:10.1039/C5RA03707G

524 Xiao H, Li J, He B (2017) Anatase-Titania Templated by Nanofibrillated Cellulose and
525 Photocatalytic Degradation for Methyl Orange. *J. Inorg. and Organomet. Polym. Mater* 27:1022–
526 1027; doi: 10.1007/s10904-017-0550-8

527 Yatsenko DA, Medvedeva TB (2019) Estimating crystallinity index of microcrystalline cellulose
528 using diffraction methods. *Journal of Structural Chemistry* 60:1430–1436; doi:
529 10.1134/S0022476619090075

530 Zdravkov A, Kudryashova J, Kanaev A, Povolotskiy A, Volkova A, Golikova E, Khimich N
531 (2015) A new solvothermal route to efficient titania photocatalyst. *Mater. Chem. Phys* 160:73–79;
532 doi:10.1016/j.matchemphys.2015.04.008

533 Zhang X, Chen YL, Liu RS, Tsai DP (2013) Plasmonic photocatalysis, *Rep. Prog. Phys* 76:
534 046401; doi: 10.1088/0034-4885/76/4/046401

535 Zlotski SV, Uglov VV (2017) Facile sol-gel synthesis of metaloxide nanoparticles in a
536 cellulose paper template *J. Nanomedicine Nanotechnology* S8:002; doi: 10.4172/2157-7439.S8-
537 002

538



[Click here to access/download
Supplementary Material
SI_Khimich_Revision_2.docx](#)

